The National Nanotechnology Infrastructure Network

Research Experience for Undergraduates (NNIN REU) Program

2009 Research Accomplishments

Space-Charge Limited Current Calculations in Nanowires

Ian Braly

Chemical Engineering, Oregon State University

NNIN REU Site: Center for Nanotechnology, University of Washington, Seattle, WA
NNIN REU Principal Investigator(s): David S. Ginger, Chemistry, University of Washington
NNIN REU Mentor(s): Obadiah Reid, Chemistry, University of Washington
Contact: bralyi@onid.orst.edu, ginger@chem.washington.edu, obadiah@gmail.com

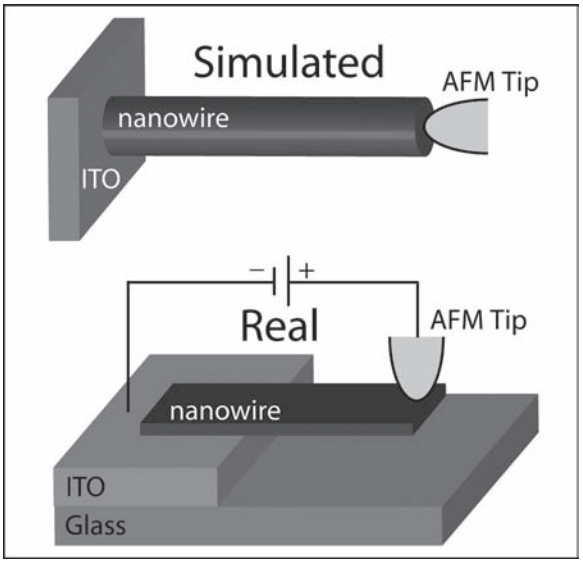

Figure 1: (top) The geometry of existing numerical models for space-charge limited current through a nanowire. (bottom) The geometry of AFM experiments on which space-charge limited currents are measured.

Abstract and Introduction:

Existing models of a space-charge limited current through a single polymer nanowire do not agree with experimental data from conductive-atomic force microscopy measurements. A better theoretical understanding of space-charge limited transport in these polymer nanowires [1] would allow for quantitative carrier mobility measurements [2]. Our hypothesis was that the disagreement between existing models and experiments was due to differences in the geometry. In this work we developed a numerical model that has a geometry conforming much more closely to that found in experimental measurements (see Figure 1). Our results suggest that the discrepancy between our models and experiments cannot be explained by this difference in geometry.

Procedure:

We used two coupled differential equations to simulate charge transport in our model: the drift-diffusion equation and the Poisson equation. The drift-diffusion equation describes how charge-carriers move through an electric field and in response to charge density gradients, while the Poisson equation describes how the electric field is affected by the charge-carriers.

We used COMSOL Multiphysics 3.5a to solve this coupled system of equations in a variety of geometries. This software solves differential equations by breaking up the geometry into smaller pieces and finding self-consistent solutions in each piece. This method is called the finite element method.

Our model development was centered on constructing a realistic geometry for the simulation. Control geometries were used in order to test that the model could reproduce understood scenarios such as the plane-parallel electrode case. Then, while only changing one element of the geometry at a time, more complicated cases (geometries) could be solved.

Results:

Figure 2 shows simulation results for the most experimentally conformal geometry we produced. The current density is much higher along the corners of the nanowire near the injection point, and then funnels towards the center of the nanowire near the extraction surface.

Figure 3 shows current-density voltage curves from an AFM experiment (circles) and our simulation (squares). The current density is dependant on the square of the injection voltage for both the experiment and the updated simulation, strongly suggesting a space-charge limited current.

Figure 4 shows current density-transport distance curves from an AFM experiment (circles), original simulation (triangles), and updated simulation (squares). Both of the simulated results show an inverse-square relationship between current density and charge-carrier transport distance. This is much different than the sub-linear dependence on length that the experimental results show.

Discussion:

It is unclear why the current density is higher at the corners in the nanowire in Figure 2. We speculate that this may not be a physical phenomenon, but rather an artifact in the simulation. This feature has been found in both the updated geometry model and in original simulations. Further investigation

is required to understand the origin of this feature, and whether it effects our results for total current density.

The dependence of current density on the square of the voltage suggests that both the simulated and experimental currents are space-charge limited (see Equation 1). There is still a lack of agreement between the experimental results from the single nanowire space-charge limited current experiment and the theoretical results from the model, even after the model geometry was made to better match the conductive-atomic force microscopy experiment. Both the original model and the updated model show a length dependence on the current density of L^{-2}. This suggests that the orientation of the atomic force microscope tip does not affect the current density's length dependence.

Conclusion:

Space-charge limited current measurements have been made in the past in order to measure the charge-carrier mobility of a single semiconducting polymer nanowire [2]. The simulations that were run in parallel to this experiment did not yield results that agreed with the experimental results. It was hypothesized that this lack of agreement was due to the model geometry not being realistic enough. We have developed a new model that reorients the atomic force microscope tip to touch the nanowire on the side of the wire instead of the end, and changes its shape from cylindrical to prism shaped.

Once the geometry was updated we verified that our model still produced a quadratic relationship between current density and voltage. This is evidence that the current remains space-charge limited. The length dependence of the current density was found to be L^{-2}. This relationship is very similar to the current density-length relationship that was found in the original model. From these results we conclude that neither the orientation of the atomic force microscope tip on the nanowire, nor the exact shape of the nanowire significantly affect the charge transport characteristics.

Further modeling of alternate geometries and investigation of the experimental conditions are required in order to explain the present discrepancy between our experiment and models.

Acknowledgements:

We thank the University of Washington NNIN Site Coordinator Ethan Allen. We thank the National Nanotechnology Infrastructure Network Research Experience for Undergraduates Program and National Science Foundation for funding.

References:

[1] H. Xin, F. Kim and S. Jenekhe. J.Am.Chem.Soc., 130(16), pp 5424-25 (2008).

[2] O. Reid, K. Munechika and D. Ginger. NanoLett., 8 (6), pp 1602-1609 (2008).

[3] A. Talin, F. Léonard, B. Swartzentruber, X. Wang, and S. Hersee, Phys. Rev. Lett., 101 (076802), 2008.

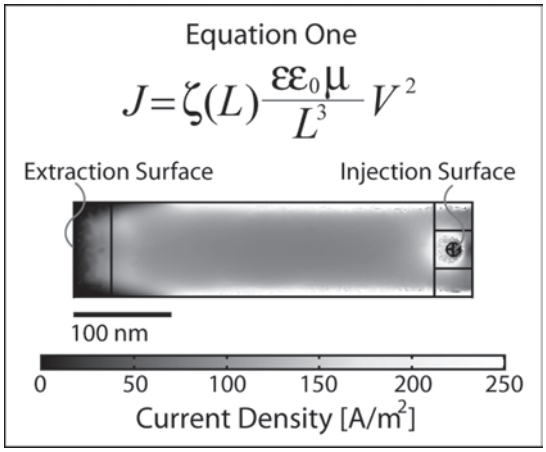

Figure 2: (top) The generalized equation for describing a space-charge limited current [3], where J is current density, ζ(L) is a geometry dependent function of length, $\varepsilon\varepsilon_0$ is the permittivity, μ is the charge-carrier mobility, V is injection voltage, and L is transport distance (wire length). (bottom) The solution of the updated model, showing current density.

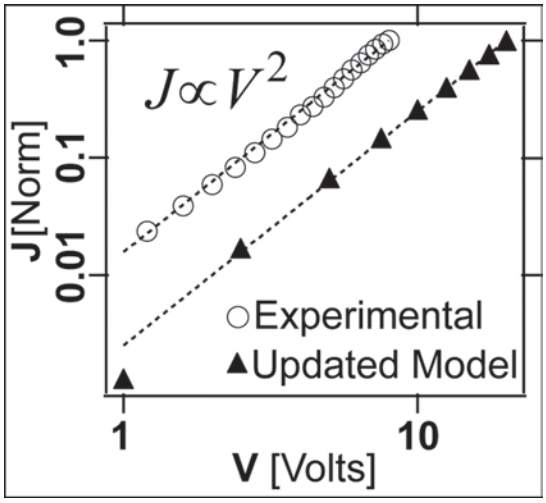

Figure 3: Current density versus injection voltage, with the experimental data (open circles), and the updated model data (closed triangles).

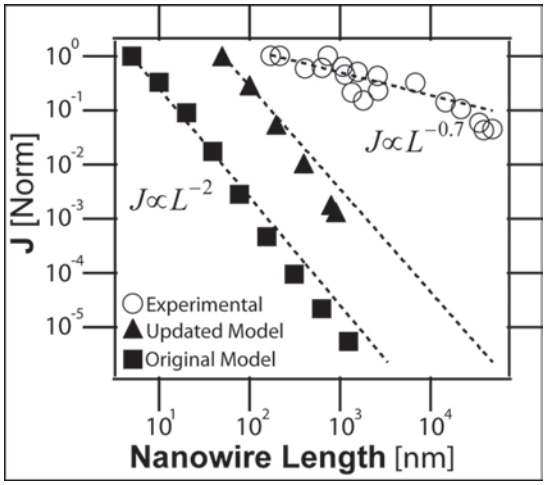

Figure 4: Current density versus wire length, with the experimental data (open circles), the updated model data (closed triangles), and the original model data (closed squares).

Raman Topography Studies of Eutectic Systems of Strontium Ruthenate and Ruthenium

Eric Hao

Engineering, University of California, Berkeley

NNIN REU Site: Penn State Nanofabrication Laboratory, Pennsylvania State University, State College, PA
NNIN REU Principal Investigator(s): Dr. Ying Liu, Department of Physics, The Pennsylvania State University
NNIN REU Mentor(s): Yiqun A. Ying, Neal Staley, Conor Puls; Physics, The Pennsylvania State University
Contact: eric_hao@berkeley.edu, liu@phys.psu.edu, yzy116@psu.edu

Abstract:

We report unexpected phenomena observed on the Sr_2RuO_4-Ru eutectic system featuring ruthenium (Ru) islands embedded in *p*-wave superconductor strontium ruthenate (Sr_2RuO_4) with a superconducting transition temperature (T_c) nearly twice that of pure Sr_2RuO_4. This enhancement of a *p*-wave superconductor is significant because of its similar structure (perovskite) compared to *d*-wave superconductors (high T_c superconductors). It occurs at the atomically sharp interface between the two materials, with the electronic states modified strongly. To examine this, we employed Raman spectroscopy, a convenient method of measuring phonon stiffness. A laser was shone onto the sample, where excited electrons scatter phonons—energy dependent on specific bonding structure—and the emitted photon was recaptured and analyzed. As we performed line scans across the interface, we noticed the phonons hardened near the interface, suggesting the T_c of the eutectic phase correlates with phonons.

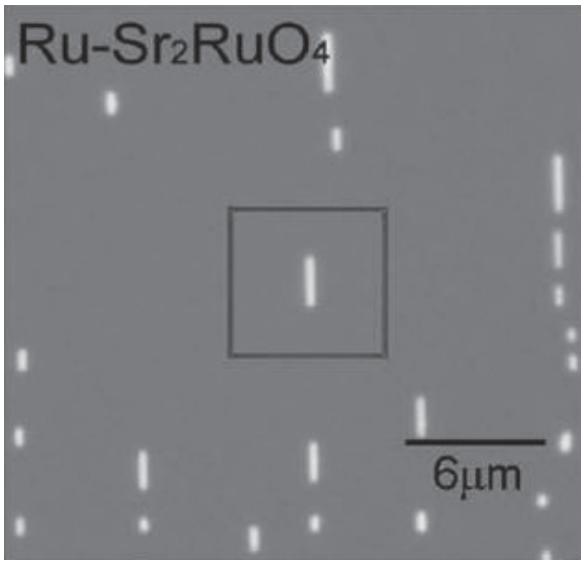

Figure 1: Eutectic system consisting of ruthenium (brightly lit areas) and Sr_2RuO_4.

Types of Superconductors:

The main theory for explaining superconductivity is the BCS Theory (named after Bardeen, Cooper, and Schrieffer), which, to put it simply, says that superconductivity relies on special electron-phonon interactions that create Cooper Pairs. If these Cooper Pairs can survive the vibrations of the crystal lattice (below a certain temperature T_c), then the material is superconducting. This theory, however, only explains the simplest type of superconductor—*s*-wave—which constitutes a majority of all superconductors. These *s*-wave superconductors typically have critical temperatures in the range of 0-10K. Another type of superconductor—*d*-wave—is well-known and studied for its high critical temperature characteristics (highest 140K); however these have extremely complicated crystal structures. The superconductor system we are interested in composes of Sr_2RuO_4—a chiral *p*-wave superconductor [1-4] that has T_c in range of *s*-wave (1.5K), but exhibits similar structure as *d*-wave—and ruthenium metal —a conventional *s*-wave superconductor (T_c = 0.5K). This eutectic system [5] is grown by adding ruthenium oxide to a strontium ruthenate substrate, with excess ruthenium forming islands about 1-2 μm in width and as long as 10 μm in length. The interface between these two materials exhibit an enhanced region of superconductivity: T_c = 3K. This is interesting because Sr_2RuO_4 usually is extremely sensitive to impurities, which destroy its superconductivity. This project aims to find evidence of crystal restructuring through use of phonon detection.

Procedure:

Raman spectroscopy discriminates materials based on bonding structure. To summarize, it works by shooting a photon at the sample, and collecting the inelastically reflected photon containing the "molecular imprint." This is quantified by measuring its resulting shift in energy.

A 514.5 nm wavelength laser, operating at 13 milliWatts of power, was shone onto a sample of the eutectic phase of

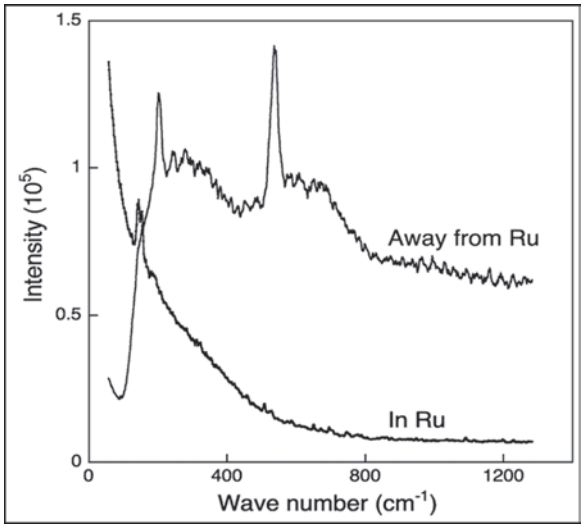

Figure 2: Spectrum of bulk ruthenium (bottom curve) and bulk Sr_2RuO_4 (top curve).

Sr_2RuO_4-Ru. Its spot size was determined using an optics formula, which came out to a 349 nm lateral resolution. First, we measured the Raman spectrum at bulk Sr_2RuO_4, which exhibited apex oxygen vibrations at 537.5 cm^{-1} and strontium vibrations at 203.11 cm^{-1}. We then measured the Raman spectrum at bulk ruthenium, which exhibited vibrations at 190 cm^{-1}. Since the enhanced phase occurs outside of the ruthenium island, we chose to measure the vibrational shift of Sr_2RuO_4.

We first performed line scans, starting at bulk Sr_2RuO_4 and moving in 349 nm increments, collecting spectra at each point, until the strontium and oxygen vibrational modes disappeared inside the ruthenium island.

Results:

We received data ranging from 50 cm^{-1} to 1300 cm^{-1}. First, we cropped out the irrelevant data, obtaining two sets (one for strontium and one for oxygen). We removed the linear bias associated with each region, and fit Gaussian peaks, recording its central peak position. We noticed a shift of about 8.3 cm^{-1} in the oxygen vibration, a change of about 1.3%, as well as a shift of about 1.6 cm^{-1} in the strontium vibration, corresponding to a change of about 0.8%. We were also successful at reproducing this phenomenon, through repeated line scans in different areas, and different islands.

Conclusion:

Raman spectroscopy data gave evidence of so-called "phonon stiffening." The change in the vibrational frequencies of both the strontium and oxygen reflected a change in the phonons associated with the crystal structure. This change in crystal structure was correlated with the change in the critical temperature of the 3K enhanced phase, suggesting that phonons play an important role in the enhancement of the eutectic system.

Further suggested experiments include temperature-dependent as well as polarization dependent Raman spectroscopy measurements in order to further quantify this "phonon stiffening."

Acknowledgments:

The author would like to thank Dr. Y. Liu; Y. A. Ying; N. Staley; C. Puls; J. Stitt; Dr. J. Robinson; Dr. R. Redwing, as well as the National Science Foundation; The NNIN REU Program; the Department of Energy; and the Department of Defense, Army Research Office for funding.

References:

[1] A. P. Mackenzie, Y. Maeno, Rev. Mod. Phys. 75, 657 (2003).
[2] K.D. Nelson, Z.Q. Mao, Y. Maeno, Y. Liu, Science 306, 1151 (2004).
[3] J. Xia, Y. Maeno, P. T. Beyersdorf, M. M. Fejer, A. Kapitulnik, Phys. Rev. Lett. 97, 167002 (2006).
[4] F. Kidwingira, J. D. Strand, D. J. van Harlingen, Y. Maeno, Science 314, 1267 (2006).
[5] Y. Maeno et al., Phys. Rev. Lett. 81, 3765 (1998).

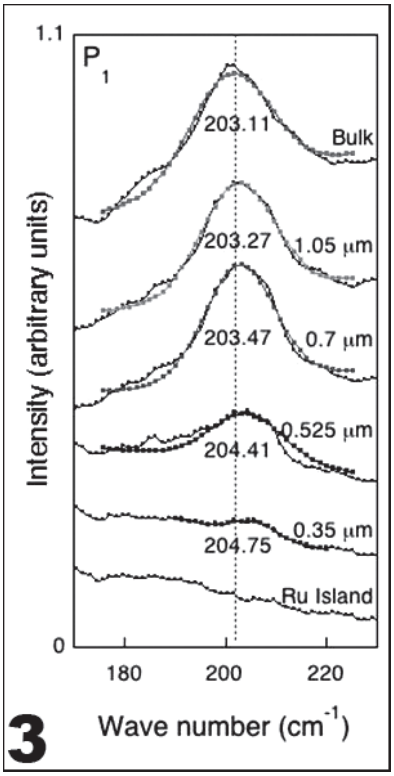

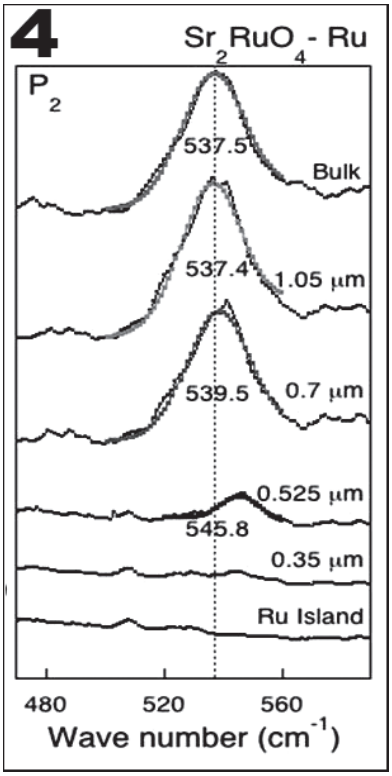

Figure 3: Sr vibration line scans with peak positions and distance from island.

Figure 4: Oxygen vibration line scans with peak positions and distance from island.

Fabrication of Sub-Micron Lateral Spin Valves

Alayne M. Lawrence
Chemical Engineering, Xavier University of Louisiana

NNIN REU Site: Nanofabrication Center, University of Minnesota-Twin Cities, Minneapolis, MN
NNIN REU Principal Investigator(s): Professor Paul Crowell, Physics, University of Minnesota-Twin Cities
NNIN REU Mentor(s): Michael Erickson, Physics, University of Minnesota-Twin Cities
Contact: alawren1@xula.edu, crowell@physics.umn.edu, erickson@physics.umn.edu

Introduction:

This research project focused on the fabrication of sub-micron lateral spin valves, which are devices consisting of two or more conducting materials that allow us to measure spin injection and relaxation in metallic structures. These spin valves modulate electrical transport depending on the alignment of two magnetic electrodes. In this case, the two magnetic electrodes are separated by a channel of a normal metal, which can be copper, silver or aluminum. One of the major problems with these spin valves is that the resistivity of the normal metal channel, which is grown by evaporation, is dominated by defects. We suspect that if we make these spin valves out of better materials then the spin lifetime will increase. Progress on the fabrication of lateral spin valves of high purity, high conductivity transport channels of copper, aluminum, and silver will be presented.

Experimental Procedure:

Different methods were employed to increase the diffusion length by reducing the resistivity using high purity wires and foils. First, we selected high purity wires and foils on which we intended to deposit ferromagnetic contacts. The aluminum, copper and silver wires used were all approximately 99.99% pure. The aluminum and copper foils were both approximately 99.999% pure and the silver sample used was approximately 99.998% pure. We then measured the residual resistivity ratio of the wires and foils before and after annealing.

Residual Resistivity Ratio:

The measurement we were most concerned with was the residual resistivity ratio (RRR). RRR is measured by the resistance of a sample at room temperature divided by the resistance at a low temperature. At a low temperature, the resistance of an ordinary metal is determined by scattering from defects, while at room temperature the resistivity is dominated by scattering from lattice vibrations. A cleaner sample will therefore have a higher RRR. (See Figure 1.)

Dunk Probe:

At first we were measuring a crude RRR number by measuring the resistance at room temperature and then measuring the resistance at 77K by dunking it into liquid nitrogen. As the measurements progressed, it was clear we needed to examine the temperature dependence of the resistivity below 77K; so in order to do so we decided to use a liquid helium dunk probe to get more accurate data.

The dunk probe works by simply attaching a sample to a large probe and then actually dunking it in a helium Dewar. Figure 2 shows data obtained using the dunk probe.

Annealing:

In order to fabricate better spin valves, we explored improving the properties of the normal metal by annealing. Annealing is a heat treatment that is used to change the grain structure of samples in order to increase the electron transport.

The first anneal was conducted in vacuum. Samples of high purity wires were placed in a quartz tube inside a furnace which was connected to a turbo-molecular pump. Inside the furnace the temperature was brought up to 350°C at a pressure of 4×10^{-6} Torr. After approximately six hours of annealing, we discovered that the RRR did not change significantly and therefore we decided to try annealing in an

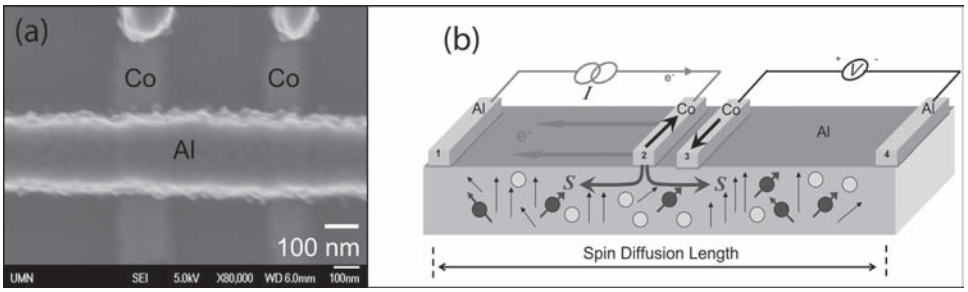

Figure 1: (a) SEM micrograph of a lateral spin valve; (b) Schematic diagram of the device.

oxygen atmosphere. The oxygen annealing was basically conducted in the same manner as the vacuum annealing; the only difference was that a furnace was connected to an oxygen tank instead of a vacuum pump. In addition, a slightly higher temperature of 400°C was used.

Photolithography:

The annealing processes were both done on high purity wires. Eventually we decided to test on high purity foils. Astonishingly, the high purity foils gave RRR's that were significantly larger. We decided to use these foils as the channel for our future spin valves. Since the foil area was very large and the channels for these devices are very small, photolithography was used to etch micron scale wires from foils.

For this process, first the high purity metal foils were mounted on a glass substrate with wax. A thin layer of photoresist (S1818) was then spun followed by a two minute soft bake at 105°C. Second, a wire was mounted onto the foil as a photolithography mask and the same resist was spun again and baked. Third, after the second soft bake was done the sample sat under an ultraviolet light for two minutes in order to keep only the small wire that we wanted. The wire was removed then the resist was developed and a wet etch was done through the metal foils so that a wire was created.

Results and Conclusions:

A comparison of the RRR's amongst different samples suggests that we can improve the transport properties of high purity metal foils. The ability to fabricate spin valves from these materials may lead to better understanding of the role of defects and grain structure on spin relaxation. Additionally SEM micrographs suggest that we may have been able to change the grain structure of metals through annealing. With this knowledge we will be able to go forth and make spin valves out of high purity materials in hope of increasing the spin lifetime. In addition, this work may serve to ultimately develop a new process to deposit ferromagnetic contacts on a single crystal wire.

Acknowledgements

I would like to acknowledge Professor Paul Crowell, Michael Erickson, Eric Garlid and Mun Chan from the Physics Department at University of Minnesota-Twin Cities. I would also like to acknowledge Christopher Leighton Lab in Materials Science at the University of Minnesota-Twin Cities. Lastly, I would like to acknowledge National Nanotechnology Infrastructure Network Research Experience for Undergraduates Program and National Science Foundation for funding.

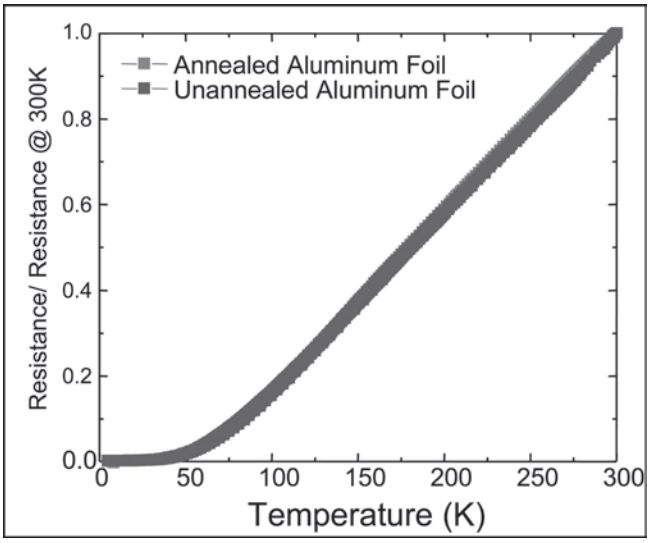

Figure 2: Typical resistivity data for an Al foil.

Sample	Unannealed	Vacuum Annealed	Oxygen Annealed
Aluminum Wire	10.554	11.455	16.203
Copper Wire	7.114	7.635	7.843
Silver Wire	5.129	5.54	5.222
	Unannealed	Annealed	
Aluminum Foil	840	1090	
Copper Foil	271	563	
Silver Foil	25	32	

Figure 3: Table of all RRR measurements.

Magneto-Transport in Photoexcited Diamond

Sarah Reiff

Physics, Marquette University

NNIN REU Site: Nanotech@UCSB, University of California, Santa Barbara, CA

NNIN REU Principal Investigator(s): Professor David Awschalom, Center for Spintronics and Quantum Computation, University of California Santa Barbara

NNIN REU Mentor(s): Joseph Heremans (2005 NNIN REU at Cornell), Center for Spintronics and Quantum Computation, University of California Santa Barbara

Contact: sarah.reiff@marquette.edu, awsch@physics.ucsb.edu, jheremans@umail.ucsb.edu

Abstract and Introduction:

Diamonds are uniquely suited for electronic and spintronic device applications. Ultrahardness, a wide band-gap of 5.5 eV, and a high thermal conductivity are ideal material properties for electronic devices requiring high power, high frequency, or high temperature. Additionally, defects in diamond are a single-spin system and single photon source, with potential for room temperature quantum computation. However, little is known about certain electrical properties in diamond. Here, we attempt to determine the carrier type and density of a single-crystal, nitrogen-rich diamond, by measuring the photoexcited Hall effect. Using a physical properties measurement system (PPMS), it is possible to take these measurements over varied temperatures and magnetic fields.

Experimental Procedure:

In this investigation, we explored single crystal, type Ib diamond, grown by the high-temperature, high-pressure method with a substitutional nitrogen concentration of 10^{19} atoms/cm^3. Using small-scale photolithography techniques and electron-beam deposition, we evaporated 100/500/900 Å of titanium/platinum/gold in a four pad Van der Pauw geometry (Figure 1). Each contact pad was 1 mm^2 and the gaps between neighboring contacts were 50 μm. The large contact pads allowed for an optical fiber to be glued to the area at the center of the pads in a process known as pig-tailing. The fiber was attached directly onto the sample with optical glue [1]. After metallization, one sample was annealed at 230°C for 36 hours to eliminate any surface conduction effects caused by hydrogen-terminated bonds.

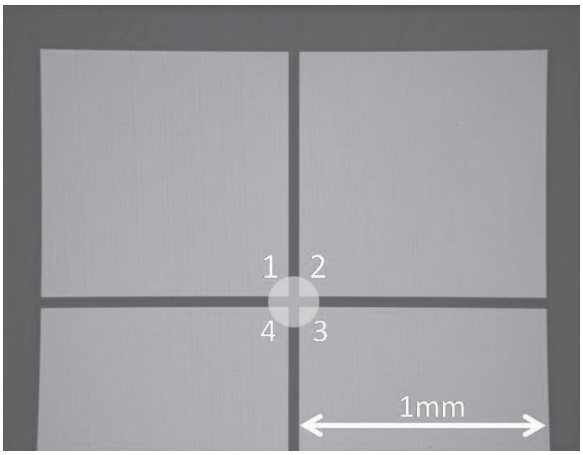

Figure 1: An optical micrograph of a diamond sample (dark color) with 1 mm x 1 mm Ti/Pt/Au contact pads (light squares). The contact pads are numbered in the Van der Pauw geometry. The lightest circle represents the photoexcited area.

The measurements were taken using a PPMS, which is a cryogenic chamber capable of cooling down to temperatures as low as 1.8 K. A superconducting electromagnet, within the PPMS, can apply magnetic fields to the sample up to 14 T normal, which is optimal for Hall effect measurements. The integrated electronics in the PPMS allow for a large array of measurement capabilities; however, it does not provide a system for optical illumination. Two modifications were critical for photoexcitation with a powerful, external laser.

First, a custom probe stick insert was designed and fabricated to lower the fiber and sample down the length of the sample chamber and into the measurement space (Figure 2 a,b). The stick was made of G-10 fiberglass with non-magnetic brass fixtures. The G-10 pieces were bonded together using cryogenic epoxy. The thermal expansion of all materials used was carefully considered for cycling from room temperature to 10 K to ensure that the stick insert remained shorter than the PPMS sample chamber.

Once the fiber was fed through the probe stick, it was pig-tailed directly onto the sample (Figure 2c). The diamond was photoexcited using a sub-bandgap 532 nm (2.3eV) laser beam which passed through a series of expansion optics and focused into a 105 μm core fiber. To withstand temperatures as low as 4.2 K, the fiber had aluminum cladding. The other end of the fiber was directed via a Teflon® ferrule out of the PPMS through the second modification: a specialized vacuum fitting consisting of a Swagelok and KF flange [2].

In our setup, the 2.3 eV laser was used to optically bridge the center region between the pads, and excite carriers from within the diamond. These nitrogen-rich diamonds have

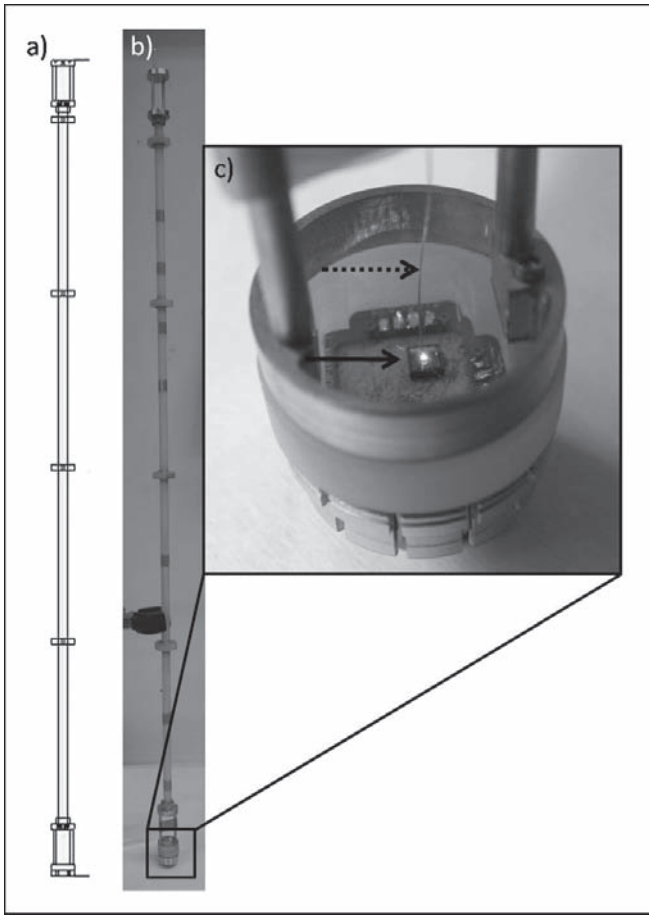

Figure 2: a) A schematic drawing of probe stick insert design. b) Image of the fabricated probe stick insert. c) View of the lower portion of stick insert including sample (solid arrow) and pigtailed optical fiber (dotted arrow).

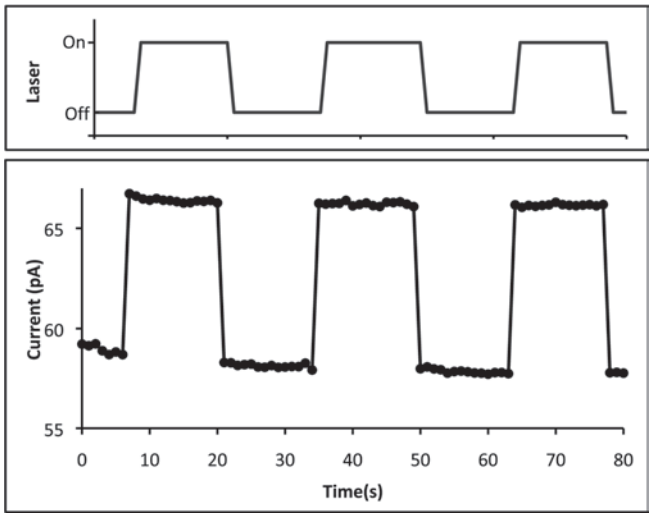

Figure 3: Plot of current (pA) and laser state vs. time (s) showing an increased current corresponding to times when the laser is used to photoexcite the sample.

shown photoinduced charge storage effects likely due to the presence of substitutional nitrogen defects, believed to reside 1.9eV below the conduction band [3]. To verify photoconductivity, the stick assembly was tested at room temperature by applying a DC voltage across two pads, between which the current was measured using a current preamplifier. Figure 3 shows the measured current between pads 2 and 4, dependent on the laser illumination as plotted on a time axis. Under illumination, there should be an increase in the current due to the excitation of carriers and a decrease when the laser is blocked. This is a successful proof of concept that the pig-tailed fiber can indeed demonstrate photoconductivity in type Ib diamond.

Conclusions:

We have demonstrated a successful photoconductivity technique using a custom designed PPMS probe stick insert and pig-tailed optical fiber on single crystal, nitrogen rich diamond. With this, we are now able to subject samples to normal incident magnetic fields of a few Tesla over a large range of temperatures. Having successfully seen photoconductivity in this system, we can begin to investigate the photoexcited Hall effect in type Ib diamond.

Acknowledgements:

I would like to thank my mentors, Joseph Heremans and Shawn Mack, my principal investigator, Prof. David Awschalom, fellow cohort, Matthew Brehove, and the rest of the Awschalom group for their constant support and guidance during the program. I would also like to thank Angela Berenstein, the UCSB REU site coordinator. This work was sponsored by the National Science Foundation, the Air Force Office of Scientific Research, and the National Nanotechnology Infrastructure Network Research Experience for Undergraduates Program.

References:

[1] F. M. Mendoza, Ph.D. thesis, UC Santa Barbara, 2008.
[2] E.R. Abraham, E.A. Cornell, Applied Optics, 37, pp.1762 (1998).
[3] F. J. Heremans, et al., Appl. Phys. Lett. 94, 152102 (2009)

Fabrication of a Stable Tunable Fabry-Perot Interferometer in the Fractional Quantum Hall Regime

Paden Roder

Physics, Grinnell College

NNIN REU Site: Center for Nanoscale Systems, Harvard University, Cambridge, MA
NNIN REU Principal Investigator(s): Dr. Charles Marcus, Physics, Harvard University
NNIN REU Mentor(s): Angela Kou, Douglas McClure; Physics, Harvard University
Contact: roderpad@grinnell.edu, marcus@harvard.edu, akou@physics.harvard.edu, dmcclure@fas.harvard.edu

Abstract:

Electronic Fabry-Perot interferometers on high mobility gallium arsenide / aluminum gallium arsenide heterostructures have recently been used in attempts to detect non-Abelian statistics in the fractional quantum Hall regime. Though successful in the integer quantum Hall regime, these devices appear to lack the electrostatic stability needed for interference measurements at fractional filling factors. This is likely due to the fact that the doping of the material is optimized for high mobility, leading to poor gateability. Here we report on the development of a new generation of devices where gates are deposited in etched trenches rather than on the surface of the chip, allowing them to operate at smaller voltages where they are more stable.

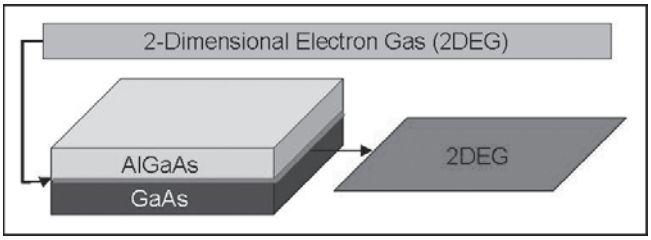

Figure 1: A two-dimensional electron gas.

Introduction:

Under exchange of identical particles, fermions have an anti-symmetric wave function whereas bosons have a symmetric wave function. This difference in symmetry properties is responsible for the characteristics of different particles, such as photons and electrons. However, particles that are neither fermionic nor bosonic, termed anyons, have been hypothesized to occur in the fractional quantum Hall regime [1]. The filling factor 5/2 has received particular attention since the anyons there are believed to be non-Abelian and therefore potential building blocks for a topological quantum computer [2].

In the Hall effect, a current in a two-dimensional (2D) electron gas (Figure 1) running orthogonal to a magnetic field generates a Hall resistance, perpendicular to both the current and the magnetic field, due to the Lorentz force. At low enough temperatures and high enough magnetic fields, quantization of the energy spectrum leads to plateaus in the Hall resistance known as the quantum Hall effect.

Furthermore, it has been observed that certain quantized Hall resistances most likely result from the formation of correlated states where charge is carried by anyonic quasiparticles whose charge is a fraction of an electron's. For these fractional quantum Hall states to form, a high-mobility 2D electron gas is required. Such a 2D electron gas can be created at the interface of a gallium arsenide/aluminum gallium arsenide heterostructure [3]. An interference device, seen in Figure 2, defined by negative voltages applied to metal gates on the surface of the chip, has been proposed to detect the non-Abelian anyons required for topological quantum computing via their effect on the relative phase of interfering trajectories. So far, a major obstacle has been the electrostatic stability of the device.

Here, etching the interferometer into the chip is explored as a possible way to reduce the needed gate voltages, possibly increasing stability.

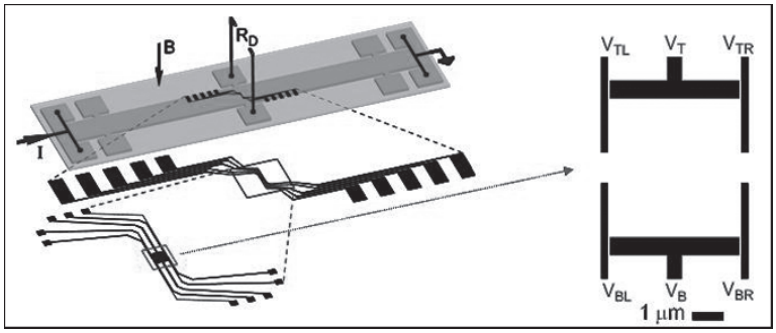

Figure 2: An electronic interferometer device is shown on typical Hall bar used in quantum Hall measurements [4].

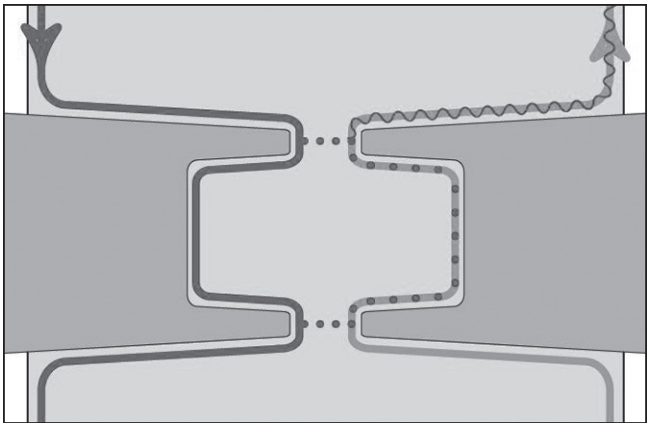

Figure 3: Charges in the two-dimensional electron gas travel along the edges of the device. Tunneling at the two quantum point contacts leads to interference [5].

Methods:

Previous fabrication methods of the electronic interferometer deposited the gates on the surface of the heterostructure. The gates' large distance to the 2D electron gas and screening from the donor layer necessitate the use of relatively large gate voltages, resulting in unstable, "switchy" device behavior. By depositing the gates in etched trenches instead of on the surface, both of these problems may be alleviated. The drawback of this method is that etching the interferometer features becomes difficult when dealing with separations of short distances (in our case, 140 nm). If etched too far, the gates could become shorted due to lateral etching. If etched too little, no advantage is observed.

In order to find the optimal fabrication parameters, multiple devices were written onto a chip using electron beam lithography at different exposure doses. After developing, the chip was then etched some distance. This procedure was repeated using multiple chips, where for each chip, the distance etched was varied. Finally, titanium/gold gates were deposited via thermal evaporation.

After fabricating devices that passed visual inspection in the scanning electron microscope, the gates were tested by measuring the device resistance as a function of gate voltage at 4 K. A sharp rise in resistance signals depletion of the 2D electron gas under the gates. Comparing the gate voltage at which depletion occurs in etched versus unetched samples provides a quantitative measure of the effect of the etching.

Results and Conclusions:

The farthest distance etched so far was 115 nm. Since the distance from 2D electron gas to the surface of the heterostructure is 200 nm, the distance to the gates is 85 nm. As seen in Figure 4, despite the etched features being connected, the gates do not short. Modeling the gates and the 2D electron gas as a parallel plate capacitor suggests that the absolute value of the depletion voltage in the etched device should be reduced by 0.386V from that in the unetched device. Experimentally, a decrease of 0.3 V is observed. However, the depletion voltage in both cases is roughly 1 V more negative than that predicted from this simple model, suggesting that screening from the donor layer may still be an issue.

Future Work:

The next set of devices can be etched farther in order to further reduce the gate voltages needed. Once an optimal etch depth is chosen, the device will be cooled in a dilution refrigerator and used for fractional quantum Hall interferometry. If the etching has led to increased stability, non-Abelian statistics may finally be observed.

Acknowledgements:

I would like to thank the Charles Marcus group, specifically my mentors Angela Kou and Douglas McClure, for providing an immense amount of guidance, knowledge, experience, and patience during the summer. Also, I would like to thank Kathryn Hollar, the Harvard CNS staff, the NSF, and the NNIN REU program for an unparalleled summer experience.

References:

[1] Wilczek, F. Fractional Statistics and Anyon Superconductivity. World Scientific, Singapore, 1990.

[2] Kitaev, A. Y. "Fault Tolerant Quantum Computation by Anyons", Annals of Physics, 303, 2- 30 (2003).

[3] Stormer, H. "Nobel Lecture: The Fractional Quantum Hall Effect" Reviews of Modern Physics, 71, 875-889 (1999).

[4] McClure, D. et al. "Edge-State Velocity and Coherence in a Quantum Hall Fabry-Perot Interferometer" (2009), arXiv:0903.5097 [5] Illustration by Douglas McClure.

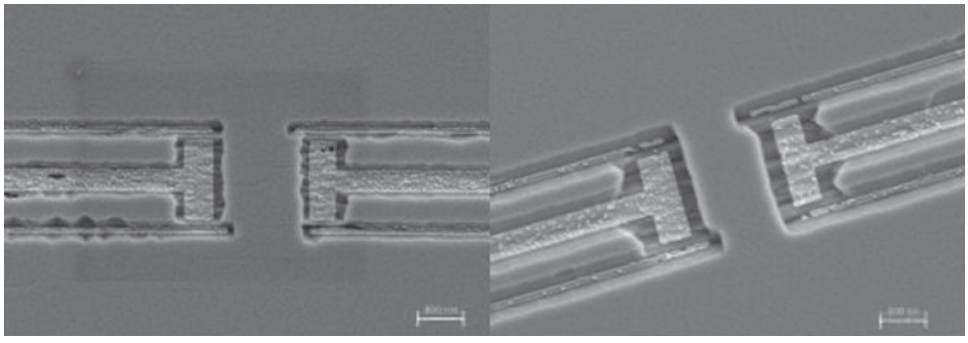

Figure 4: The left device is etched ~ 60 nm and the right device is etched ~ 115 nm.